Published in final edited form as:
*Nat Geosci*. 2019 September ; 12(9): 696–700. doi:10.1038/s41561-019-0398-3.

# Early Moon formation inferred from Hafnium-Tungsten systematics

**Maxwell M. Thiemens**[1,*], **Peter Sprung**[1,2], **Raúl O. C. Fonseca**[1], **Felipe P. Leitzke**[3], **Carsten Münker**[1]

[1]Institut für Geologie und Mineralogie, Universität zu Köln, Germany

[2]Hot Laboratory Division (AHL), Paul Scherrer Institut, Villigen, Switzerland

[3]Steinmann Institut, Universität Bonn, Germany

## Abstract

The date of the Moon-forming impact places an important constraint on Earth's origin. Lunar age estimates range from about 30 Myr to 200 Myr after solar system formation. Central to this age debate is the greater abundance of $^{182}$W inferred for the silicate Moon than for the bulk silicate Earth. This compositional difference has been explained as a vestige of less late accretion to the Moon than the Earth, following core formation. Here we present high-precision trace element composition data from inductively coupled plasma mass spectrometry for a wide range of lunar samples. Our measurements show that the Hf/W ratio of the silicate Moon is higher than that of the bulk silicate Earth. By combining these data with experimentally derived partition coefficients, we find that the $^{182}$W excess in lunar samples can be explained by the decay of now extinct $^{182}$Hf to $^{182}$W. $^{182}$Hf was only extant for the first 60 Myr after solar system formation. We conclude that the Moon formed early, approximately 50 Myr after the solar system, and that the excess $^{182}$W of the silicate Moon is unrelated to late accretion.

The Moon likely formed in the aftermath of a giant impact between the proto-Earth and an erstwhile planetary body1. Extreme chemical and isotopic similarities between the Earth and the Moon2 have led to a growing consensus that Earth and Moon share a common chemical ancestry. This similarity in chemical signatures implies either that the bulk silicate Earth (BSE) is the major source of Moon-forming impact debris3–6 or that proto-Earth and the impactor had virtually identical chemical compositions6. Beyond chemical constraints on the Moon forming giant impact event, there is an ongoing controversy regarding its exact



[*]**Corresponding Author** Correspondence and requests for materials or further information should be addressed to M.M. Thiemens, at MaxwellMT@gmail.com, Laboratoire G-Time, Département Géosciences, Environnement et Société, Université Libre de Bruxelles.

**Data Availability Statement**: The authors declare that the data supporting the findings of this study are available within the article and its supplementary information files.

**Contributions** MT and CM did the sample digestions, column chemistry, and the HFSE-W-U-Th ID concentration measurements partially supported by PS on the Neptune MC-ICP-MS at Cologne. PS, ROCF, and FL did the modelling based on experimental partitioning data. MMT did the modelling relating Hf/W to $^{182}$W. All authors contributed towards the writing of the manuscript and the discussion of the implications of the data.

**Competing Interests** The authors declare no competing interests.


Europe PMC Funders Author Manuscripts

timing, with some researchers arguing that the Moon formed early (i.e., 30 to 100 Myrs after Solar System formation – SSF)7–12, whereas others contend the Moon formed up to 200 Myrs after SSF13–17. Constraining lunar formation requires knowing the crystallization age of the lunar magma ocean (LMO), a product of the Moon's high-energy impact formation. Central to the lunar age controversy are small excesses in the $^{182}$W abundance in lunar basalts when compared to the Earth, which average a value of 25 $\mu^{182}$W units18–20. Assuming that the excess $^{182}$W in lunar samples stems from the in situ decay of short-lived $^{182}$Hf to $^{182}$W (8.9 Myrs half-life21) would place lunar formation between 30 and 60 Myrs after SSF when sufficient $^{182}$Hf was still present. However, this interpretation is at odds with the apparent observation that BSE and the silicate Moon have virtually overlapping ratios of Hf (mother) to W (daughter), with Hf/W ratios of 24.9 and 25.8, respectively22,23. These apparently identical parent to daughter ratios imply that their different $\mu^{182}$W cannot be related to the *in situ* decay of $^{182}$Hf. Hence, an alternate explanation invoked that Earth and Moon received a disproportionate contribution of late accretion components with a chondritic Hf/W ratio (~1) and lower $^{182}$W than BSE19. Because the Moon is less massive than Earth, it would have received a commensurately smaller contribution from late accretion, and has thus retained a higher $\mu^{182}$W than BSE18–20. The Moon therefore constitutes a suitable highly-siderophile element (HSE) poor end-member in such late accretion models and a possible analogue to a proto-Earth that was essentially devoid of late accretion components20. In addition to this view, the apparent decrease in $^{182}$W values measured in terrestrial rocks over geologic time has been explained by the protracted mixing of late veneer material into the terrestrial mantle that lowered $\mu^{182}$W to its present-day value12,20,24,25. The presence of negative $^{182}$W anomalies in Archaean samples, however, preclude the origin of $^{182}$W excess entirely from late accretion26. Often, the $^{182}$W anomalies that have been found are coupled with $^{142}$Nd anomalies, which is a decay product of $^{146}$Sm, both lithophile elements24,26–29, making it likely that $^{182}$W excesses are the result of early silicate differentiation events.

Any accurate interpretation of lunar $^{182}$W data relies on an accurate knowledge of the Hf/W ratio value in lunar mantle reservoirs and by inference of the silicate Moon. Unfortunately, lunar Hf-W systematics are poorly constrained, as data of sufficient precision are scarce. This also extends to other highly incompatible elements (e.g., HFSE, U and Th) that are commonly used as proxies for W behaviour during dry terrestrial mantle melting23. In previous lunar studies33, W was treated as a perfectly incompatible element (i.e., having a similar behaviour as U or Th) during lunar differentiation. This treatment might be incorrect, as lunar mantle melting occurs under more reducing conditions than in the terrestrial mantle, implying that W may behave less incompatibly than elements like U and Th30–32. In fact, previous observations show that ratios of W with U or Th appear to be variable in lunar samples, which suggests that W behaves differently to highly incompatible elements like U or Th during lunar magmatism33, in agreement with recent experimental studies30–32.

## Apollo sample results

To provide robust constraints on the Hf/W ratio value of the silicate Moon, we performed high-precision concentration measurements of W, Th, U, and other high field strength elements (HFSE) by isotope-dilution on a representative sample suite covering most relevant

lithological units on the lunar nearside. Our samples include low- and high-Ti basalts, ferroan-anorthosites (FAN), and KREEP-rich rocks. As shown in Figure 1, these groups of samples are compositionally distinct, as expected from radiogenic isotope evidence and geochemical modelling34. Low-Ti mare basalts display a narrow range in U/W and Hf/W ratios between 1.5 and 2.5 and between 30 and 50, respectively. In contrast, high-Ti basalts have Hf/W ratio as high as 150, and slightly more fractionated U/W, with values between 0.5 and 2.2. Finally, the KREEP-rich rocks and FAN samples exhibit the lowest Hf/W range of the studied sample suite, between ca. 5 (FAN) and 23 (KREEP-rich), while their U/W shows the largest range amongst all samples, with values approaching zero for FAN and as high as 3.5 for the KREEP-rich rocks.

## Lunar source modelling

Several key observations can be derived from our high precision W-U-Th-HFSE data. For example, when combined, the FAN and KREEP-rich rocks form a clear linear array in Hf/W ratio vs. U/W space (Fig. 1). This array can directly be linked to early lunar crust formation, i.e., likely the result of mixing between a FAN end-member that has an exceedingly low Hf/W and U/W, and a KREEP-like component having elevated U/W and a Hf/W of around 20 (i.e., lower than both bulk silicate Moon and Earth's mantle). Interestingly, our results for these KREEP-rich samples corroborate previously modelled U/W and Hf/W values for KREEP using a $fO_2$-sensitive set of partition coefficients30, which predicted that KREEP has an elevated U/W and a lower Hf/W ratio value than the bulk silicate Moon depending on $fO_2$. Our data thus show that the LMO crystallization model35, as well as the mineral/melt partitioning data24,25 used here, are sufficiently robust for mass balancing these elements.

Our new results for lunar mare basalts have the best potential to constrain the Hf/W ratio of the silicate Moon. In defining which lunar mantle reservoirs of LMO cumulates were involved in the genesis of mare basalts, radiogenic Hf-Nd isotope data are the most powerful proxies to constrain their source mineral assemblages34. These source mineral assemblages allow us to model the geochemical relation between basalt and mantle compositions for trace elements of interest. For example, Hf-Nd isotope data can clearly identify late-crystallizing mare basalt sources comprising Ti-rich oxide phases and clinopyroxene, a characteristic that is absent from low-Ti mare basalt source regions34. Even at the low $fO_2$ of the lunar mantle, such oxide phases and clinopyroxene preferentially incorporate Hf over W and U31,36. Moreover, the mantle source of the Apollo 17 high-Ti mare basalts is the most likely lunar mantle source to contain residual metal during partial melting, owing to its reduced nature30,31. Residual metal in lunar mantle sources would undoubtedly retain W and not Hf, and thus generate higher Hf/W ratio in co-existing mare basalts. When modelling high-Ti mare basalts with small fractions of residual metal, the high-Ti samples that exhibit the highest Hf/W ratio in our sample suite are perfectly reproduced (see melting curves shown in red in Figure 1). The extreme Hf/W ratio displayed by Apollo 17 high-Ti mare basalts, and their co-variation with U/W (Figure 1), therefore directly reflect the combined effects of residual Ti-rich oxides, pyroxene, and metal in the mantle sources of Apollo 17 high-Ti basalts. An unfortunate consequence of this feature is that any inferred U-W-Hf pattern strongly depends on the degree of partial melting that is not well

constrained for Apollo 17 basalts. Thus, Apollo 17 high-Ti mare basalts cannot be reliably used to infer the Hf/W ratio of the bulk silicate Moon, as done previously18.

In contrast to the sample types above, the sources of low-Ti mare basalts are straightforward to model, as these are not overprinted by KREEP components and are essentially devoid of both Ti-rich oxides and metal34 that may fractionate W from U, Th, or HFSE. . Moreover, low-Ti basalts are thought to result from higher-degrees of partial melting compared to high-Ti basalts37–40, and the U/W and Hf/W ratio measured in these basalts should be virtually identical to those in their respective sources. Interestingly, there are clearly resolvable differences between the different groups of low-Ti basalt samples (Figure 1). This heterogeneity in Hf/W ratio and U/W values in distinct low-Ti mantle sources is in perfect agreement with the isotopic heterogeneity documented by previously published Hf-Nd isotope data34. Moreover, these variations in Hf/W ratio and U/W observed in our lunar samples are consistent with previous experimental studies that predict that W is less incompatible than Hf during LMO crystallization and partial melting of lunar mantle cumulates30,31.

The mafic cumulates that constitute the mantle sources of low-Ti basalts are expected to preferentially retain W over Hf and U during LMO crystallization at reducing conditions (crystal/silicate melt partitioning values shown in supplementary materials). Therefore, the LMO cumulates, and by inference, the measured Hf/W ratio of low-Ti lunar mantle sources (30.2 to 48.7) record minimum estimates of the Hf/W ratio in the bulk LMO as well as of the silicate Moon. Altogether, our data therefore show that the Hf/W ratio of the silicate Moon must lie between 30 and 50, clearly higher than the value estimated for the BSE (25.8 ± 2.6)23. As the addition of late veneer material would lower the lunar Hf/W ratio, the minimum estimate of the Hf/W ratio remains a robust one, being still resolvably higher than the Hf/W ratio of the BSE. In summary, low-Ti mare basalts allow the most reliable Hf/W ratio estimates in the lunar mantle, and the Hf/W ratio of the lunar mantle can be clearly shown to be resolvably higher than that of Earth’s mantle.

## Lunar formation scenarios

Figure 2 illustrates three scenarios that can explain the higher Hf/W in the lunar mantle: A first, traditional scenario (Fig. 2a) explains the different Hf/W ratios by variable proportions of added late veneer. It has been suggested by several studies18–20 that the Moon received a considerably lower proportion of late veneer than the BSE. The lower $\mu^{182}W$ and Hf/W ratio of the BSE are then explained by the addition of a higher amount of unradiogenic W through late accretion to the Earth than to the Moon. In a second scenario (Fig. 2b), the Moon forming event could have taken place amidst ongoing terrestrial core formation, when $^{182}Hf$ was still present. If the Moon formed that early, core formation has certainly been taking place at more reducing conditions than during its final stages40,41. Under such more reducing conditions, the Hf/W ratio of BSE at the time of the giant impact would have been higher than at present, because W would have been more efficiently extracted into the growing core40. This model obviates the need for late accretion to explain the lunar excess in $\mu^{182}W$, because the Moon preserved a higher Hf/W ratio than the silicate Earth, leading to less radiogenic $\mu^{182}W$ in the BSE and more radiogenic $\mu^{182}W$ in the silicate Moon. In

the third scenario (Fig. 2c), core formation in the Moon could have scavenged sufficient W into the lunar core to elevate the Hf/W ratio of BSM to its higher present-day value. This process has been invoked previously to explain the depletion of Cr and siderophile elements in the lunar mantle42,43, with additional losses through evaporation44. If the lunar core, and by inference the Moon, formed while $^{182}$Hf was extant, the silicate Moon would inevitably develop $^{182}$W higher than the present day terrestrial value. Collectively, the two last scenarios imply that late accretion was either of no consequence to the W budget and isotope composition of the silicate Moon, or that it was contemporaneous to the Moon forming event.

A simple strategy to further evaluate the three models described above is to test the simplest hypothesis to explain why the Hf/W ratio of the silicate Moon is higher than that of BSE, i.e., lunar core formation (model III). If lunar core formation will raise the Hf/W ratio of the silicate Moon to values as high as those shown here (i.e., 30-50), then the first two hypotheses are potentially superfluous. While there is plenty of evidence that the Moon has a small core, its exact composition and formation conditions are not well understood. However, the mass of the lunar core is much better constrained. Based on a recent re-evaluation of lunar seismic data45–47 the lunar core comprises 1-3 % of the total mass of the Moon. The question remains whether such a small core could have scavenged sufficient W to shift the Hf/W ratio of the silicate Moon to values as high as reported here. A simple mass balance48 can be made to model the Hf/W ratio of the silicate Moon after lunar core formation. This model assumes that Hf is perfectly lithophile, and that its abundance in the bulk Moon and the BSE are identical. The Hf-W contents of the modelled silicate Moon can be calculated assuming closed-system core formation, over a range of realistic $D_W^{core/mantle}$ (15-100), initial Hf/W ratio of BSE (25.8), and different core mass fractions (1-3 %). We also include a historical, lower estimate for the BSE49. The results of the modelling are depicted in Figure 3, showing that that lunar core formation can indeed reproduce the range of Hf/W ratio of the lunar mantle if one assumes $D_W^{core/mantle}$ higher than 60, and a core mass fraction of at least 1.5%, i.e., in line with recent estimates45–47. A more massive core (3% mass fraction), would permit smaller $D_W^{core/mantle}$ (ca. 30) to reproduce the Hf/W ratio range of 30-50 reported here. It is thus clear from the results of this model that lunar core formation can viably generate the Hf/W ratio of BSM using realistic values of $D_W^{core/mantle}$ and core mass fractions48.

## Implications for dating lunar formation

While the presence of a lunar core helps settle the $^{182}$W excess, there remains evidence from other radiometric dating systems for a young Moon. Evidence from direct measurements such as zircons and FAN ages can provide a younger age, but may be long offset from the parent body age13–15,24. Amongst these, our suggested age concurs with the oldest age found via U-Pb, at 4.51 Ga7. Other methods, such as Sm-Nd model ages, have indicated a young age for lunar crust formation, varying from 4.35 to 4.45 Ga based on lunar basalts15 and KREEP13,17. However, the age implied by these samples is for lunar crust formation, rather than for lunar formation. Importantly, the Sm-Nd model ages can represent post-formation mantle processes which may have reset the different isotope systems.

In conclusion, we prefer a simple model for the lunar Hf-W patterns, wherein the difference in Hf/W ratio between the silicate Moon and the silicate Earth is the result of lunar core formation. Figure 4 illustrates variations of lunar $^{182}W$ systematics as a function of Hf/W ratio and age. The range of Hf/W ratio measured in our study, combined with recent estimates for the lunar $\mu^{182}W$ requires lunar differentiation to have occurred between 40.5 and ca. 60 Myrs after SSF. We can thus unambiguously relate the $^{182}W$ excess in lunar samples to in-situ decay of $^{182}Hf$ to $^{182}W$. The combination of a robust set of experimental partitioning data with high precision HFSE analysis is thus in favour of an “old Moon,” while simultaneously diminishing the role of late accretion in creating the $\mu^{182}W$ signature of the Moon. In addition to helping settle the ongoing strife between “old” and “new” Moon scenarios, this method can also be used to unravel formation timescales of other planetary bodies, being of key importance to future sample return missions.

## Methods

### 1 Sample selection

Samples were provided by the Curation and Analysis Planning Team for Extraterrestrial Materials (CAPTEM), and selected to represent the major lithological units of the Moon as sampled by the NASA Apollo missions. Characterizing their chemical composition, our particular focus lay on the quantification of any inherent U/W, Th/W, and Hf/W variability as inferred from the few previous studies available. Some sample duplicity with previous studies allows for an additional quality assessment. In total, lunar samples from Apollo 11 (3), Apollo 12 (6), Apollo 14 (3), Apollo 15 (6), Apollo 16 (4), and Apollo 17 (4) were analyzed. Of these, 7 were Apollo 11 or Apollo 17 high-Ti mare basalts and soils, 14 were low-Ti mare basalts from Apollo 12 and 15, 2 Apollo 16 ferroan-anorthosites (FAN), as well as 7 KREEP-rich samples including a meteorite and KREEP-rich breccias and KREEP-basalts from the Apollo 14, 16, and 17 missions.

### 2 Sample Preparation

To obtain high precision data, we measured all elements of interest by isotope dilution and added several isotope tracers to ca. 100 mg (250 mg for anorthosites) of each sample prior to digestion. The mixed isotope tracers included $^{229}Th$-$^{233}U$-$^{236}U$ and $^{183}W$-$^{180}Ta$-$^{180}Hf$-$^{176}Lu$-$^{94}Zr$ mixed solutions. Samples were digested in 3 ml of double distilled HF and 3 ml of distilled $HNO_3$ for 24 hours at 120 °C. Prior to drydown, 0.5 ml of perchloric acid were added to ensure sample-spike equilibrium for Th. Samples were re-dissolved with concentrated $HNO_3$ and trace HF to ensure re-dissolution of HFSE. These sample solutions were subsequently dried down again, and re-dissolved in 6 ml 6 M HCl-0.06 M HF to ensure full sample-spike equilibrium for HFSE. These samples were then aliquoted, with 10% of the solution being used for conventional trace element analysis, 20% for W isotope dilution measurements, and 70% for high field strength and U-Th element analysis. For a first batch of samples, an additional aliquot of 10% for U-Th was taken. The anorthosite samples were aliquoted with 85% to a combined HFSE, W, and U-Th aliquot, and 15% for trace element analysis.

The trace element aliquot was dried down, dissolved in concentrated $HNO_3$, and then dried down again. This residue was subsequently dissolved in 1 ml concentrated $HNO_3$, with 4 ml MQ $H_2O$ added, and then diluted with MQ $H_2O$ to 50 ml. Conventional trace elements on these aliquots were performed at the Quadrupole ICP-MS laboratory at the Institut für Geowissenschaften at CAU zu Kiel using the procedure of ref. 50.

Our protocol for separating individual HFSE and U-Th cuts from lunar samples is a modified protocol based on refs 22,51,52. During the protocol, individual cuts containing a matrix, HRRE, Zr-Nb, Ta, Hf and U-Th were separated from the HFSE aliquot. Tungsten was separated from the W isotope dilution step via a separate set of anion exchange resin microcolumns (after ref. 52, Table 4).

In our HFSE protocol, the sample aliquots were dissolved in 3N HCl and loaded onto a Ln Spec resin column. Matrix and LREE were eluted in 3M HCl. An HREE fraction containing most Lu was eluted with 6N HCl, followed by elution of an HFSE cut containing Ti-Zr-Nb-Hf-Ta-U-Th in 2N HF. A quantitative Zr/Nb aliquot was taken from this fraction (see ref. 51). The remaining HFSE cut was loaded onto a Bio-Rad column containing AG 1 x8 100-200 mesh resin. The U-Th fraction was collected in 2N HF, and a Ti-Zr-Hf fraction was collected in 6N $HNO_3$/0.2N HF. A clean Ta fraction was subsequently collected in 6N $HNO_3$/0.2N HF/1%$H_2O_2$. The Ti-Zr-Hf fraction was dried down overnight and loaded onto the stage I Ln Spec resin column in 3 N HCl. After cleanup in 6N HCl and MQ $H_2O$, Ti was eluted using a 1N $HNO_3$ 2% - $H_2O_2$ mixture (ref. 53), and some Zr in 6N HCl -0.06N HF. Hafnium was finally eluted in 2N HF.

Separation of U-Th was performed in two ways, following a modified protocol of (54). For the first batch of samples, a full aliquot was used, whereas for the other batches the U-Th fraction from the 2N HF elution step above was taken. After drydown, the U and Th bearing cuts were dissolved in 1.5N $HNO_3$, before being loaded onto columns containing TRU-Spec resin (200-400 mesh). Modifying the chemistry of (54), all major elements were initially eluted in 1.5N $HNO_3$. After removal of rare earth elements in HC3N HCl, Th was subsequently eluted in 0.2N HCl. Finally, U was eluted in 0.1N HCl/0.3N HF.

Given the low concentrations of the elements of interest in anorthosites, we performed a different separation protocol for these samples. Ca. 70% of the 85% HFSE aliquots of anorthosites were loaded on anion exchange resin in 1N HCl/0.5N HF solution. The eluted matrix cut and an additional fraction rinsed in 0.5N HCl/0.5NHF contained most of the Rb-Sr, Sm-Nd and U-Th. A fraction containing Ti/Zr/Hf was collected in 6NHCl/0.06NHF, from which Hf was further purified using Ln Spec resin (see above). A W fraction was subsequently eluted in 6N $HNO_3$/0.2N HF, followed by Ta elution in 6 N $HNO_3$ / 0.2N HF / 1% $H_2O_2$. After drydown, the Ta cut was loaded on the same anion resin column again for cleanup, and the Ta was again eluted in 6N $HNO_3$/0.2N HF / 1% $H_2O_2$ after cleanup in 6N $HNO_3$/0.2N HF. The remaining 15% of the anorthosite HFSE aliquots were loaded on Ln Spec resin in 3N HCl. Two fractions containing HREE and Zr/Nb werde eluted from the column in 6N HCl and 2N HF as described above. The advantage of this approach is that a larger W fraction is collected, thus avoiding low sample-to-blank ratios during W ID measurements.

## 3 Analytical protocols

All isotope dilution measurement were performed using the Neptune MC-ICP-MS at Cologne. Detailed descriptions of the analytical protocols for HFSE measurements, analytical uncertainties and further references are given in (22). For $^{229}Th/^{232}Th$ measurements, we used an SEM ion counter equipped with an RPQ system on mass $^{229}Th$. The Th cuts were doped with the NBL CRM 112A U standard for mass bias correction, and the ion counter was calibrated with concentration-matched IRM-035 and IRM 036 standards for ion counter yield corrections. For U measurements, mass bias was corrected using the measured $^{233}U/^{236}U$ of the spiked U cuts and the certified $^{233}U/^{236}U$ from (55) for the doped IRM-3636 double spike that was used for preparation of the mixed U-Th tracer. Our external precision and accuracy for elemental ratios determined by isotope dilution involving U and Th typically is better than ±1% for both U/W and Th/W (2σ r.s.d.). Typical blanks during the course of the measurements were below 50 pg for W, 66 pg for U, 32 pg for Th, and 30 pg for Hf. These blanks proved negligible, with total blank-uncertainty-including propagated errors of less than ±1%.

## 4 Results (and modeling constraints)

Measured HFSE and HFSE/U-Th ratios are distinct for different sample groups and mineralogy, with only small variations in U/W and Hf/W between samples from the same lithology. High-Ti basalts are particularly heterogeneous, with samples from the three measured localities showing distinct Hf/W and U/W values. Apollo 17 High-Ti breccias both have similar values, with Hf/W ranging from 31 to 35, at a constant U/W of 1.9. This is distinct from Apollo 17 high-Ti mare basalts, where U/W correlates positively with Hf/W. The Apollo 11 high-Ti mare basalts both have Hf/W of 42 and U/W of 2.2. Unique amongst all samples are the Apollo 17 high-Ti mare basalts, which bear exceptionally high Hf/W ratios, between 120 and 150. Likewise, the low-Ti basalts plot as particularly distinctive groups according to mission site. The Apollo 12 ilmenite basalts have similar U/W to the Apollo 12 olivine and pigeonite basalts, of 2.07 and 2.25, respectively. However, they are distinct in their Hf/W, with both pigeonite-bearing basalts near 30 and ilmenite-basalts of 43-48. The Apollo 15 quartz-normative and olivine-normative low-Ti basalts have different U/W, ranging from an average of 2.45 in the former to 1.75 in the latter. The Hf/W of the two low-Ti basalt groups also vary from 45 (quartz-normative) to 30 (olivine normative). Whereas the olivine-normative low-Ti basalts of both Apollo 15 and Apollo 12 have identical Hf/W, their U/W differ significantly, from amongst the lowest values (1.63) measured to the highest (2.53). The KREEP-rich samples have a very narrow range in Hf/W of ca. 20. The U/W of KREEP samples has the largest spread, with most samples ranging from 1.63 to 2.51, and minimum and maximum values of 0.54 and 3.38, respectively.

## 5 Lunar Magma Ocean fractionation and partial melting modelling

The Lunar Magma Ocean (LMO56–58) crystallization model utilized in this study is based on the cumulate crystallization sequence of (35). We have previously shown30 that the results of this and other LMO crystallization models (e.g., refs 59,60) are in good agreement. The same starting composition used in (30) after (22) was chosen to evaluate the general HFSE-W-U-Th systematics of a crystalizing LMO. For W, an

additional mass balance between the estimate of its content in the bulk silicate Moon after core formation was done following (43), considering different core mass fractions (1-3% of the total mass of the Moon). The LMO crystallization model is divided into four main steps: (i) equilibrium crystallization of olivine and orthopyroxene (until 78% solidification), (ii) fractional crystallization of plagioclase, olivine, and pigeonite (until 86% solidification), (iii) fractional crystallization of clinopyroxene, plagioclase, and pigeonite (until 95% solidification), and (iv) crystallization of pigeonite, plagioclase, clinopyroxene, and ilmenite (until 99.5% solidification). The remaining 0.5% after LMO crystallization is a liquid residue strongly enriched in incompatible trace elements and called urKREEP, which reflects its characteristic enrichments in K, REE, and P61,62. The LMO crystallization model assumes that various amounts of trapped instantaneous residual liquid (TIRL, i.e. coexisting melt at the time of crystallization) are part of lunar mantle cumulates in order to take into account major element variation observed in lunar mare basalts35. The model also considers that at the moment plagioclase appears on the liquidus, 98% of the crystallizing plagioclase floated to the uppermost portion of the LMO to form the lunar crust with only 2% being entrained in the cumulates, in order to account for the Al content of lunar basaltic samples35. Following LMO crystallization, the layered lunar mantle underwent a density driven mantle overturn which mixed the different cumulate layers, producing new hybrid mantle domains that served as the source for partial melts that crystallized to form the lunar mare basalts63. To understand the implications of these processes for the trace element inventory of mare basalts thus involved aggregate modal fractional melting models of hybrid lunar mantle domains. The mixing proportions of different primary LMO cumulates in the hybridized lunar mantle sources, their mineral assemblages, as well as the amount of trapped instantaneous residual liquid (TIRL) were constrained from the Lu–Hf and Sm–Nd isotope patterns of lunar basalts34. We have also assumed that a small proportion of residual metal may be required at the lunar mantle source to reproduce the values observed for high-Ti basalts, which is in agreement with the extremely reduced nature of the lunar mantle and the depletion in Ni observed for lunar olivine64,65. A lunar magma ocean equilibrated at ca. IW −1 was assumed throughout the entire modelling, in agreement with the current estimates of oxygen fugacity for the lunar mantle65,66. Trace element crystal/silicate melt partition coefficients for different pyroxenes, plagioclase, and olivine (see supplemental materials) were selected taking into account the variation of $TiO_2$ exhibited by lunar mare basalts and the changing composition of the LMO during crystallization (see ref. 32) as well as the effect of $fO_2$ on the partitioning behaviour of W (see ref. 30,31). Ilmenite/silicate melt trace element partition coefficients are an average of the high-Ti experiments listed in (36). Liquid metal/silicate melt W partition coefficients are from Righter et al. (2010) and (43), which cover a wide range of values (15-100).

## Supplementary Material

Refer to Web version on PubMed Central for supplementary material.

## Acknowledgements

MMT and CM acknowledge funding through the European Commission by ERC grant 669666 “Infant Earth.” MMT acknowledges funding from Deutsche Forschungsgemeinschaft (DFG) Projekt number 213793859 (SP 1385/1-1 to PS) and EoS project ET-HOME (present funding); ROCF acknowledges funding for a Heisenberg

Fellowship by the DFG through grant DFG FO 698/5-1 and FO 698/6-1; PS acknowledges funding from UoC emerging fields grant “ULDETIS”. F.P.L. acknowledges funding for a PhD. scholarship by DAAD/CNPq (248562/2013-4). CAPTEM thanked and acknowledged for sample allocations.

## References

1. Canup RM. Forming a Moon with an Earth-like Composition via a Giant Impact. Science. 2012; 338: 1052–1055. DOI: 10.1126/science.1226073 [PubMed: 23076098]
2. Melosh HJ. New approaches to the Moon’s isotopic crisis. Phil Trans R Soc A. 2014; 372 doi: 10.1098/rsta.2013.0168 [PubMed: 25114301]
3. Zhang J, Dauphas N, Davis AM, Leya I, Fedkin A. The proto-Earth as a significant source of lunar material. Nature Geoscience. 2012; 5: 251–255.
4. Weyer S, Anbar AD, Brey GP, Münker C, Mezger K, Woodland AB. Iron isotope fractionation during planetary differentiation. Earth Planet Sci Lett. 2005; 240: 251–264.
5. Armytage R, Georg R, Williams H, Halliday A. Silicon isotopes in lunar rocks: Implications for the Moon’s formation and the early history of the Earth. Geochim Cosmochim Acta. 2012; 77: 504–514.
6. Dauphas N, Burkhardt C, Warren PH, Fang-Zhen T. Geochemical arguments for an Earth-like Moon-forming impactor. Phil Trans R Soc A. 2014; 372 doi: 10.1098/rsta.2013.0244 [PubMed: 25114316]
7. Barboni M, Boehnke P, Keller B, Kohl IE, Schoene B, Young ED, McKeegan KD. Early formation of the Moon 4.51 billion years ago. Science Advances. 2017; 3: e1602365. doi: 10.1126/sciadv.1602365 [PubMed: 28097222]
8. Jacobson SA, Morbidelli A, Raymond SN, O’brien DP, Walsh KJ, Rubie DC. Highly siderophile elements in Earth’s mantle as aclock for the Moon-forming impact. Nature. 2014; 508: 84. [PubMed: 24695310]
9. Yin Q-Z, Zhou Q, Li Q-L, Li X-H, Liu Y, Tang G-Q, Krot AN, Jenniskens P. Records of the Moon-forming impact and the 470 Ma disruption of the L chondrite parent body in the asteroid belt from U-Pb apatite ages of Novato (L6). Meteoritics & Planetary Science. 2014; 49: 1426–1439.
10. Bottke W, Vokrouhlický D, Marchi S, Swindle T, Scott E, Weirich J, Levison H. Dating the Moon-forming impact event with asteroidal meteorites. Science. 2015; 348: 321–323. [PubMed: 25883354]
11. Yin Q, Jacobsen SB, Yamashita K, Blichert-Toft J, Télouk P, Albarède F. A short timescale for terrestrial planet formation from Hf–W chronometry of meteorites. Nature. 2002; 418: 949–952. [PubMed: 12198540]
12. Moynier F, Yin QZ, Irisawa K, Boyet M, Jacobsen B, Rosing MT. Coupled $^{182}$W-$^{142}$Nd constraint for early Earth differentiation. Proc Natl Acad Sci. 2010; 107: 10810–10814. DOI: 10.1073/pnas.0913605107 [PubMed: 20534492]
13. Carlson RW, Borg LE, Gaffney AM, Boyet M. Rb-Sr, Sm-Nd and Lu-Hf isotope systematics of the lunar Mg-suite: the age of the lunar crust and its relation to the time of Moon formation. Phil Trans R Soc A. 2014; 372 (2014) doi: 10.1098/rsta.2013.0246 [PubMed: 25114305]
14. Connelly J, Bizzarro M. Lead isotope evidence for a young formation age of the Earth–Moon system. Earth and Planetary Science Letters. 2016; 452: 36–43.
15. Borg LE, Connelly JN, Boyet M, Carlson RW. Chronological evidence that the Moon is either young or did not have a global magma ocean. Nature. 2011; 477: 70. [PubMed: 21849974]
16. Snape JF, Nemchin AA, Bellucci JJ, Whitehouse MJ, Tartèse R, Barnes JJ, Anand M, Crawford IA, Joy KH. Lunar basalt chronology, mantle differentiation and implications for determining the age of the Moon. Earth and Planetary Science Letters. 2016; 451: 149–158.
17. Borg LE, Gaffney AM, Shearer CK. A review of lunar chronology revealing a preponderance of 4.34–4.37 Ga ages. Met & Planet Sci. 2015; 50: 715–732.
18. Kruijer TS, Kleine T. Tungsten isotopes and the origin of the Moon. Earth Planet Sci Lett. 2017; 475: 15–24.
19. Kruijer TS, Kleine T, Fischer-Gödde M, Sprung P. Lunar tungsten isotopic evidence for the late veneer. Nature. 2015; 520: 534–537. [PubMed: 25855296]

20. Touboul M, Puchtel IS, Walker RJ. Tungsten isotopic evidence for disproportional late accretion to the Earth and Moon. Nature. 2015; 520: 530–533. DOI: 10.1038/nature14355 [PubMed: 25855299]
21. Vockenhuber C, Oberli F, Bichler M, Ahmad I, Quitte G, Meier M, Haliday AN, Lee DC, Kutschera W, Steier P, Gehrke RJ, et al. New Half-Life Measurement of $^{182}$Hf: Improved Chronometer for the Early Solar System. Phys Rev Lett. 2004; 93: 172501–1–172501–4. [PubMed: 15525068]
22. Münker C. A high field strength element perspective on early lunar differentiation. Geochim Cosmochim Acta. 2010; 74: 7340–7361.
23. König S, Münker C, Hohl S, Paulick H, Barth A, Lagos M, Pfänder J, Büchl A. The Earth's tungsten budget during mantle melting and crust formation. Geochim Cosmochim Acta. 2011; 75: 2119–2136.
24. Rizo H, Walker R, Carlson R, Touboul M, Horan M, Puchtel I, Boyet M, Rosing MT. Preservation of Earth-forming events in the tungsten isotopic composition of modern flood basalts. Geochim Cosmochim Acta. 2016; 175: 319–336. [PubMed: 27174983]
25. Willbold M, Elliott T, Moorbath S. The tungsten isotopic composition of the Earth's mantle before the terminal bombardment. Nature. 2011; 477: 195–198. [PubMed: 21901010]
26. Puchtel IS, Blichert-Toft J, Touboul M, Horan MF, Walker RJ. The coupled $^{182}$W-$^{142}$Nd record of early terrestrial mantle differentiation. Geochem Geophys Geosys. 2016; 17: 2168–2193.
27. Mundl A, Touboul M, Jackson MG, Day JM, Kurz MD, Lekic V, Helz RT, Walker RJ. Tungsten-182 heterogeneity in modern ocean island basalts. Science. 2017; 356: 66–69. [PubMed: 28386009]
28. Jones TD, Davies DR, Sossi PA. Tungsten isotopes in mantle plumes: Heads it's positive, tails it's negative. Earth Planet Sci Lett. 2019; 506: 255–267.
29. Puchtel IS, Blichert-Toft J, Touboul M, Walker RJ. $^{182}$W and HSE constraints from 2.7 Ga komatiites on the heterogeneous nature of the Archean mantle. Geochim Cosmochim Acta. 2018; 228: 1–26.
30. Fonseca ROC, Mallmann G, Sprung P, Sommer JE, Heuser A, Speelmanns IM, Blanchard H. Redox controls on tungsten and uranium crystal/silicate melt partitioning and implications for the U/W and Th/W ratio of the lunar mantle. Earth Planet Sci Lett. 2014; 404: 1–13.
31. Leitzke FL, Fonseca ROC, Michely LT, Sprung P, Münker C, Heuser A, Blanchard H. The effect of titanium on the partitioning behavior of high-field strength elements between silicates, oxides and lunar basaltic melts with applications to the origin of mare basalts. Chem Geol. 2016; 440: 219–238.
32. Leitzke FP, Fonseca ROC, Sprung P, Mallmann G, Lagos M, Michely LT, Münker C. Redox dependent behaviour of molybdenum during magmatic processes in the terrestrial and lunar mantle: Implications for the Mo/W of the bulk silicate Moon. Earth Planet Sci Lett. 2017; 474: 503–515.
33. Palme H, Rammensee W. The significance of W in planetary differentiation processes: Evidence from new data on eucrites. Lunar and Planetary Science Conference Proceedings. 1982; 12: 949–964.
34. Sprung P, Kleine T, Scherer EE. Isotopic evidence for chondritic Lu/Hf and Sm/Nd of the Moon. Earth Planet Sci Lett. 2013; 380: 77–87.
35. Snyder GA, Taylor LA, Neal CR. A chemical model for generating the sources of mare basalts: Combined equilibrium and fractional crystallization of the lunar magmasphere. Geochim Cosmochim Acta. 1992; 56 (10) 3809–3823.
36. Dygert N, Liang Y, Hess P. The importance of melt $TiO_2$ in affecting major and trace element partitioning between Fe–Ti oxides and lunar picritic glass melts. Geochim Cosmochim Acta. 2013; 106: 134–151.
37. Day JM, Walker RJ. Highly siderophile element depletion in the Moon. Earth Planet Sci Lett. 2015; 423: 114–124. DOI: 10.1016/j.epsl.2015.05.001 [PubMed: 34465923]
38. Day JM, Pearson DG, Taylor LA. Highly siderophile element constraints on accretion and differentiation of the Earth-Moon system. Science. 2007; 315 (5809) 217–219. [PubMed: 17218521]

39. Day J, Puchtel I, Walker R, James O, Taylor L. Osmium Abundance and Isotope Systematics of Lunar Crustal Rocks and Mare Basalts. Lunar Planet Sci Conf. 2008; 39: 1071.
40. Wade J, Wood BJ. Core formation and the oxidation state of the Earth. Earth Planet Sci Lett. 2005; 236 ((1–2)) 78–95.
41. Wood B, Walter M, Wade J. Accretion of the Earth and segregation of its core. Nature. 2006; 441 (7095) 825–833. [PubMed: 16778882]
42. Walter M, Newsom H, Ertel W, Holzheid A. Siderophile Elements in the Earth and Moon: Metal/Silicate Partitioning and Implications for Core Formation. Origin of the Earth and Moon. 2000. 265–289.
43. Steenstra E, Rai N, Knibbe J, Lin Y, van Westrenen W. New geochemical models of core formation in the Moon from metal-silicate partitioning of 15 siderophile elements. Earth Planet Sci Lett. 2016; 441: 1–9.
44. Sossi PA, Moynier F, van Zuilen K. Volatile loss following cooling and accretion of theMoon revealed by chromium isotopes. Proc Natl Acad Sci. 2018; 115: 10920–10925. DOI: 10.1073/pnas.1809060115 [PubMed: 30297398]
45. Weber RC, Lin P-Y, Garnero EJ, Williams Q, Lognonne P. Seismic Detection of the Lunar Core. Science. 2011; 331: 309–312. [PubMed: 21212323]
46. Khan A, Pommier A, Neumann G, Mosegaard K. The lunar moho and the internal structure of the Moon: A geophysical perspective. Tectonophysics. 2013; 609: 331–352.
47. Garcia RF, Gagnepain-Beyneix J, Chevrot S, Lognonné P. Very Preliminary Reference Moon Model. Phys Earth Planet Int. 2011; 188 (1) 96–113.
48. Rai N, van Westrenen W. Lunar core formation: new constraints from metal-silicate partitioning of siderophile elements. Earth Planet Sci Lett. 2014; 388: 343–352.
49. Newsom H, Sims KWW, Noll PD, Jaeger WL, Maehr SA, Beserra TB. The depletion of tungsten in the bulk silicate earth: Constraints on core formation. Geochim Cosmochim Acta. 1996; 60: 1155–1169.
50. Garbe-Schönberg C-D. Simultaneous determination of thirty-seven trace elements in twenty-eight international rock standards by ICP-MS. Geostandards and Geoanalytical Research. 1993; 17: 81–97.
51. Münker C, Weyer S, Scherer EE, Mezger K. Separation of high field strength elements (Nb, Ta, Zr, Hf) and Lu from rock samples for MC-ICPMS measurements. Geochem Geophys Geosyst. 2001; 2 doi: 10.1029/2001GC000183
52. Kleine T, Mezger K, Palme H, Münker C. The W isotope evolution of the bulk silicate Earth: constraints on the timing and mechanisms of core formation and accretion. Earth Planet Sci Lett. 2004; 228: 109–123.
53. Bast R, Scherer EE, Sprung P, Fischer-Gödde M, Stracke A, Mezger K. A rapid and efficient ion-exchangechromatography for Lu–Hf, Sm–Nd, and Rb–Srgeochronology and the routine isotope analysis of sub-ng amounts of Hf by MC-ICP-MS. Journal of Analytical Atomic Spectrometry. 2015; 30: 2323–2333.
54. Luo XM, Rehkämper D-C, Lee AN. Halliday High precision $^{230}Th/^{232}Th$ and $^{234}U/^{238}U$ measurements using energy filtered ICP magnetic sector multiple collector mass spectrometry. Int J Mass Spectrom Ion Processes. 1997; 171: 105–117.
55. Richter S, Eykens R, Kühn H, Aregbe Y, Verbruggen A, Weyer S. New average values for the $n(^{238}U)/n(^{235}U)$ isotope ratios of natural uranium standards. International Journal of Mass Spectrometry. 2010; 295: 94–97.
56. Smith JV, Anderson AT, Newton RC, Olsen EJ, Wyllie PJ, Crewe AV, Isaacson MS, Johnson D. Petrologic history of the moon inferred from petrography, mineralogy, and petrogenesis of Apollo 11 rocks. Geochim Cosmochim Acta Supplement. 1970; 1: 897–925.
57. Warren PH. The magma ocean concept and lunar evolution. Annual Review of Earth Planet Sci Lett. 1985; 13: 201–240.
58. Wood JA, Dickey JS, Marvin UB, Powell BN. Lunar anorthosites and a geophysical model of the moon. Geochim Cosmochim Acta Supplement. 1970; 1: 965.

59. Elardo SM, Draper DS, Shearer CK. Lunar magma ocean crystallization revisited: bulk composition, early cumulate mineralogy, and the source regions of the highlands mg-suite. Geochim Cosmochim Acta. 2011; 75: 3024–3045.

60. Elkins-Tanton LT, van Orman JA, Hager BH, Grove TL. Re-examination of the lunar magma ocean cumulate overturn hypothesis: melting or mixing is required. Earth Planet Sci Lett. 2002; 196: 239–249.

61. Meyer C Jr, Brett R, Hubbard NJ, Morrison DA, McKay DS, Aitken FK, Takeda H, Schonfeld E. Mineralogy, chemistry, and origin of the KREEP component in soil samples from the Ocean of Storms. Proceedings of the Lunar Science Conference. 1971; 2: 393–411.

62. Warren PH, Wasson JT. The Origins of KREEP. Reviews of Geophysics. 1979; 17: 73–88.

63. Hess PC, Parmentier EM. A model for the thermal and chemical evolution of the Moons interior: implications for the onset of mare volcanism. Earth Planet Sci Lett. 1995; 134: 501–514.

64. Karner J, Papike JJ, Shearer CK. Olivine from planetary basalts: Chemical signatures that indicate planetary parentage and those that record igneous setting and process. Am Min. 2000; 88: 806–816.

65. Nicholis M, Rutherford MJ. Graphite oxidation in the Apollo 17 orange glass magma: Implications for the generation of a lunar volcanic gas phase. Geochim et Cosmochim Acta. 2009; 73 (19) 5905–5917.

66. Papike JJ, Karner JM, Shearer CK. Comparative planetary mineralogy: Valence state partitioning of Cr, Fe, Ti, and V among crystallographic sites in olivine, pyroxene, and spinel from planetary basalts. American Mineralogist. 2005; 90: 277–290.

67. Righter K, Pando KM, Danielson L, Lee CT. Partitioning of Mo, P and other siderophile elements (Cu, Ga, Sn, Ni Co, Cr, Mn, V and W) between metal and silicate melt as a function of temperature and silicate melt composition. Earth and Planet Sci Lett. 2010; 291: 1–9.



Europe PMC Funders Author Manuscripts

Europe PMC Funders Author Manuscripts

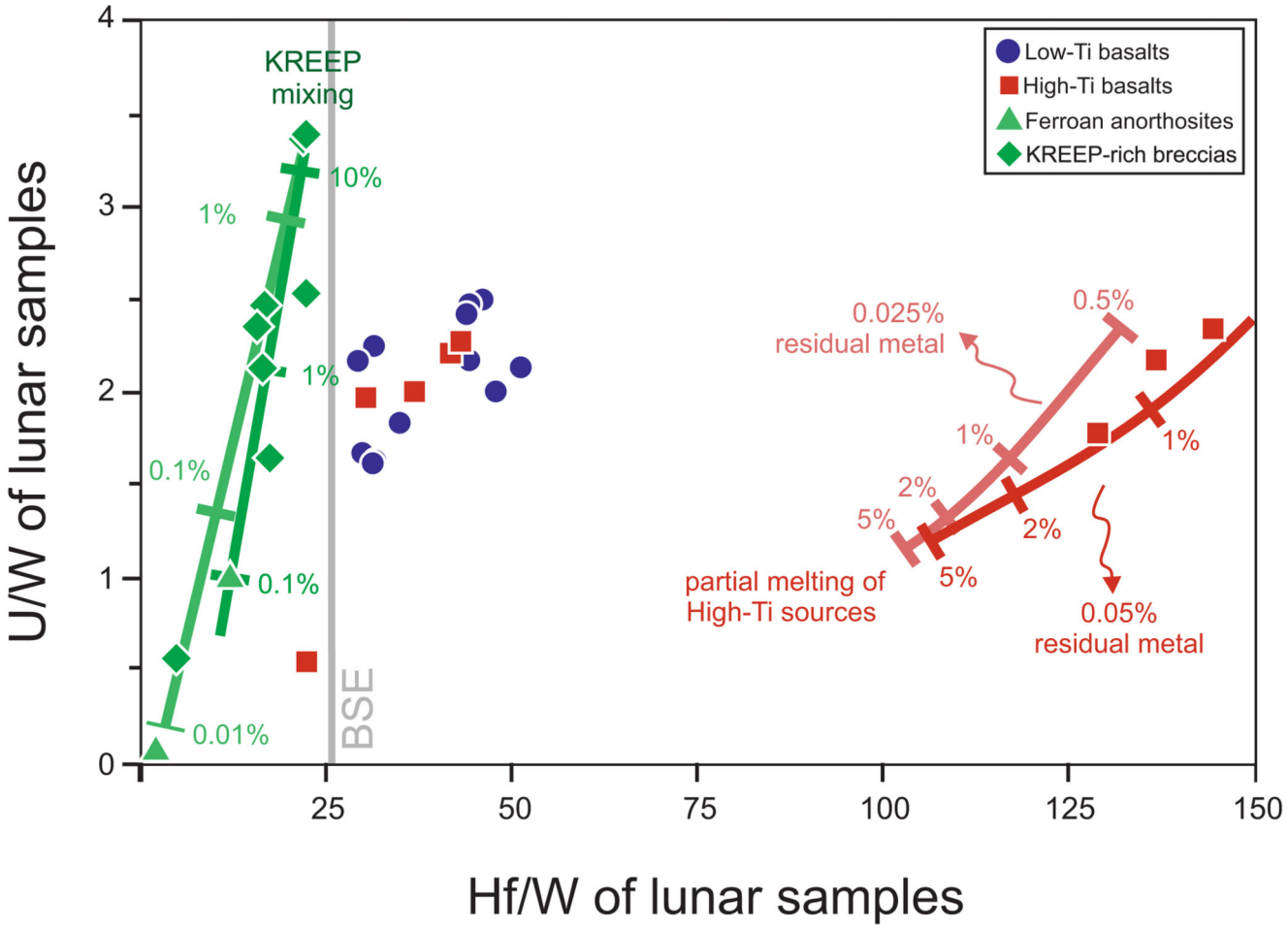


**Figure 1.**

New U/W vs. Hf/W data measured in lunar samples compared to crystallization and melting models for the LMO34. Errors are less than symbol sizes. Measured lunar highland breccia compositions straddle mixing lines between a KREEP-enriched end-member30 and FAN compositions as determined in this study. Contamination with W-rich meteoritic components produces virtually identical trajectories and raises absolute W content. The high-Ti mare basalt source mineral assemblage is defined by a mixture of LMO cumulates matching Apollo 17 mare basalt Hf and Nd isotope systematics12,27,30–32,34. Note the overall excess of Hf/W in lunar basalts compared to recent BSE estimates23.

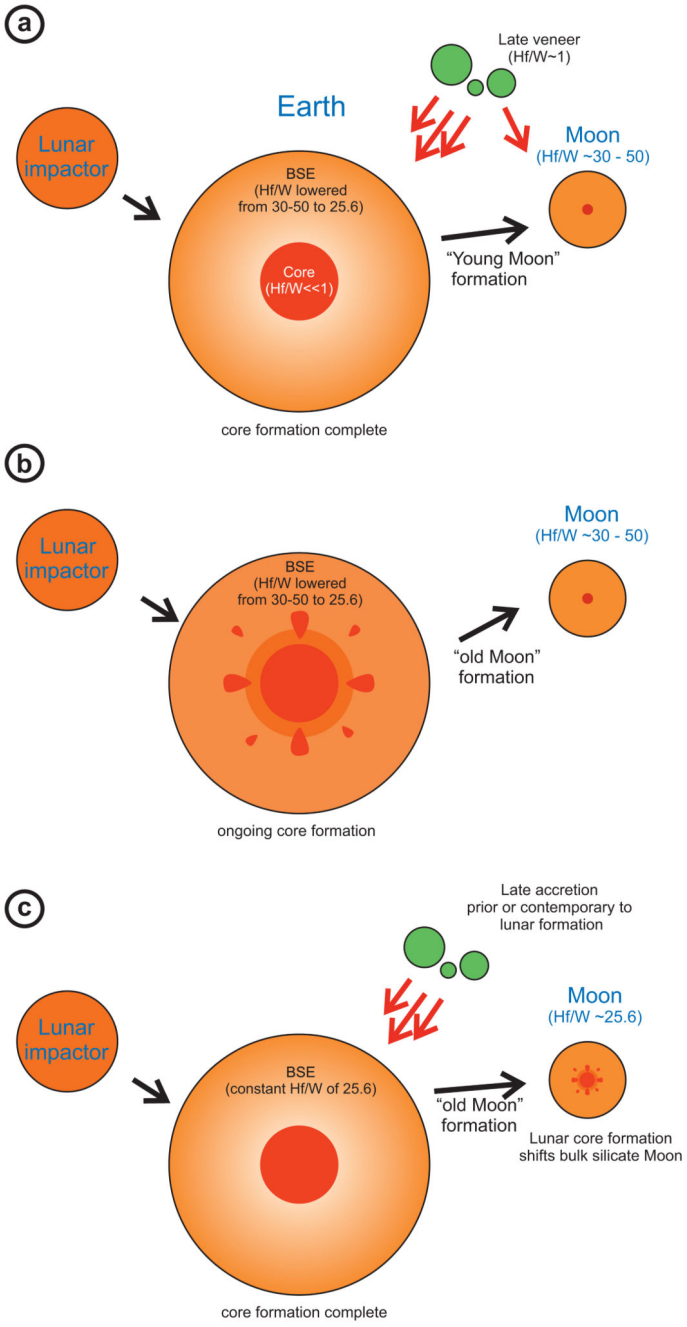


**Figure 2.**

Scenarios accounting for the higher Hf/W of the BSM. (a) A late veneer of chondritic material (Hf/W ratio~1) lowers BSE Hf/W from ca. 30-50 to 25.6 after $^{182}$Hf extinction, while the Moon preserves its original Hf/W. (b) The Moon forming event takes place while Earth's core is still forming and $^{182}$Hf is extant. Increasingly oxidised conditions later lower BSE Hf/W. (c) Formation of a small lunar core scavenged W from the BSM, increasing its Hf/W. In models (b) and (c), formation of the Moon must have occurred during the lifetime of $^{182}$Hf, i.e., within 60 Myrs after solar system formation.

Europe PMC Funders Author Manuscripts

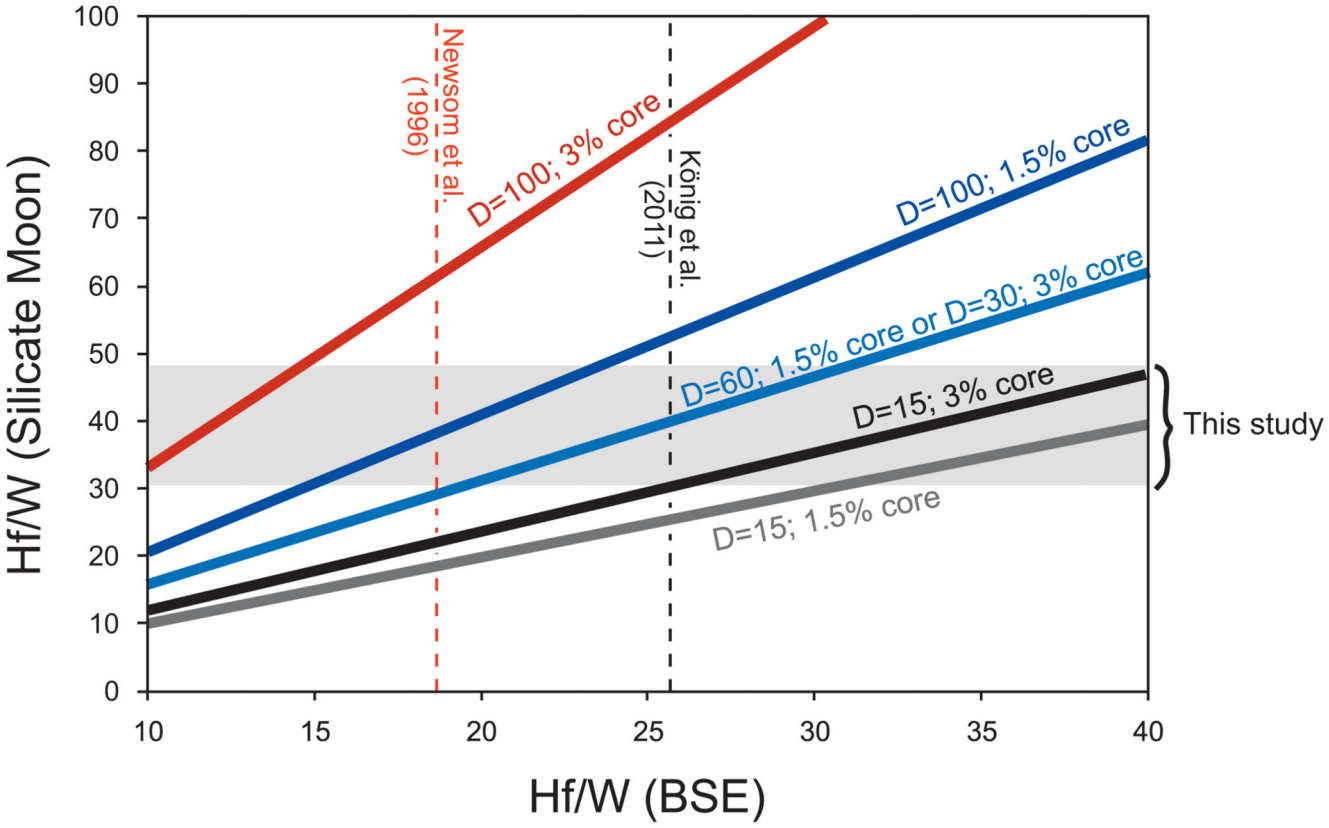


**Figure 3.**

The effect of lunar core formation on the Hf/W ratio of the silicate Moon. The models assume different metal–silicate partition coefficients for W ($D_W^{core/mantle}$ between 15–100), and different lunar core mass fractions (1.5–3%). The initial Hf/W of the Bulk Moon is the same as that of the Bulk Silicate Earth. The lunar Hf/W ratio value is reached with $D_W^{core/mantle}$ values between 30 and 60, and core mass fractions between 1 to 3% of the mass of the Moon. The two estimates of the BSE Hf/W encompass a historical value (ref. 49) and a revised value based on high precision measurements of Ta and W (ref. 23)

Europe PMC Funders Author Manuscripts

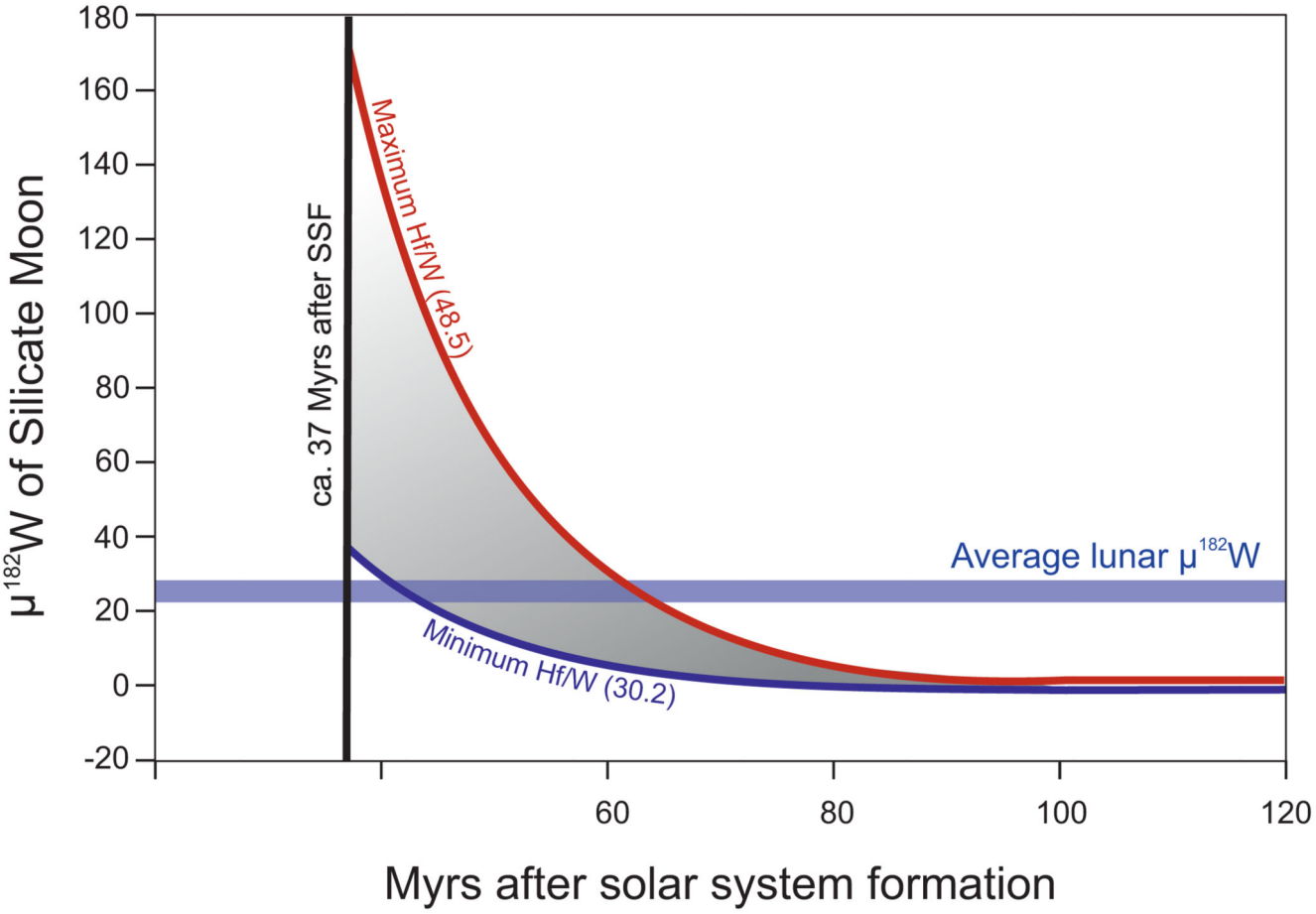


**Figure 4.**

Tungsten isotope composition ($\mu^{182}W$) of the silicate Moon as a function of the lunar Hf/W ratio and formation age. Low-Ti mare basalts proxy for the range of the BSM Hf/W. The intersection with the mean reported BSM pre-exposure $\mu^{182}W$ provides the age interval at which the Moon must have formed to explain its $\mu^{182}W$ difference to Earth by in-situ decay of $^{182}Hf$. The aggregated $\mu^{182}W$ is from ref. 18. The starting age of the curves (37 Myrs) is taken from ref. 23, as core formation ages from protracted core formation or incomplete equilibration models yield a younger age than this.